AGU PUBLICATIONS

Geophysical Research Letters

RESEARCH LETTER
10.1002/2014GL060905

Key Points:
- GRACE data recorded postseismic increase of the gravity field by 6 μGal
- Viscoelastic relaxation and afterslip were examined with the gravity data
- The GRACE data constrain the biviscous rheology model for the asthenosphere

Supporting Information:
- Readme
- Figures S1 and S2

Correspondence to:
S.-C. Han,
shin-chan.han@nasa.gov

Citation:
Han, S.-C., J. Sauber, and F. Pollitz (2014), Broadscale postseismic gravity change following the 2011 Tohoku-Oki earthquake and implication for deformation by viscoelastic relaxation and afterslip, *Geophys. Res. Lett.*, *41*, 5797–5805, doi:10.1002/2014GL060905.

Received 17 JUN 2014
Accepted 29 JUL 2014
Accepted article online 1 AUG 2014
Published online 18 AUG 2014

Broadscale postseismic gravity change following the 2011 Tohoku-Oki earthquake and implication for deformation by viscoelastic relaxation and afterslip

Shin-Chan Han[1], Jeanne Sauber[1], and Fred Pollitz[2]

[1]Planetary Geodynamics Laboratory, NASA Goddard Space Flight Center, Greenbelt, Maryland, USA, [2]U.S. Geological Survey, Menlo Park, California, USA

Abstract The analysis of GRACE gravity data revealed postseismic gravity increase by 6 μGal over a 500 km scale within a couple of years after the 2011 Tohoku-Oki earthquake, which is nearly 40–50% of the coseismic gravity change. It originates mostly from changes in the isotropic component corresponding to the M_{rr} moment tensor element. The exponential decay with rapid change in a year and gradual change afterward is a characteristic temporal pattern. Both viscoelastic relaxation and afterslip models produce reasonable agreement with the GRACE free-air gravity observation, while their Bouguer gravity patterns and seafloor vertical deformations are distinctly different. The postseismic gravity variation is best modeled by the biviscous relaxation with a transient and steady state viscosity of 10^{18} and 10^{19} Pa s, respectively, for the asthenosphere. Our calculated higher-resolution viscoelastic relaxation model, underlying the partially ruptured elastic lithosphere, yields the localized postseismic subsidence above the hypocenter reported from the GPS-acoustic seafloor surveying.

1. Introduction

The great (M_w 9.1) 11 March 2011 Tohoku-Oki earthquake disturbed not only the ground and ocean surface but also the Earth's gravity field permanently. It generated transient seismic and tsunami waves and produced large coseismic stress change that led to gradual stress redistribution and subsequent postearthquake crustal motions. The dense geodetic data such as GPS, interferometric synthetic aperture radar, and acoustic seafloor measurements reported coseismic displacement (a few tens of meters of horizontal motion and a few meters of vertical motion) and rapid postseismic displacement that yielded 10% of the equivalent seismic moment of the main shock in 2 weeks [*Ozawa et al.*, 2011; *Sato et al.*, 2011; *Simons et al.*, 2011]. Additionally, the gravitational effect of the earthquake has been measured through changes of instantaneous relative motions of two Gravity Recovery And Climate Experiment (GRACE) satellites coorbiting around 500 km altitude [*Han et al.*, 2011]. Subsequently, the time series of monthly GRACE gravity field data have been processed by optimizing the signal over the earthquake region [*Matsuo and Heki*, 2011; *Cambiotti and Sabadini*, 2012, 2013; *Wang et al.*, 2012b; *Han et al.*, 2013].

Most of the large earthquakes are followed by seismic or aseismic sliding (afterslip) on the coseismic fault and its lateral extension, by viscoelastic flow as a process of gradual relaxation of coseismic stresses, and/or by deformation induced by pore fluid migration in response to coseismic stresses [e.g., *Cohen*, 1999; *Wang et al.*, 2012a; *Hu et al.*, 2014]. *Diao et al.* [2013] inverted the postseismic GPS displacement data over the 1.5 years after the 2011 Tohoku-Oki earthquake for afterslip and viscoelastic relaxation models, and concluded afterslip is a dominant process while viscoelastic relaxation is responsible for only 11% of the postseismic moment. However, they did not evaluate biviscous processes that may explain transient deformation during the first few months as well as afterslip. For example, after the 2004 Sumatra-Andaman earthquake, in addition to GPS displacement data at teleseismic distances [*Pollitz et al.*, 2006], the GRACE gravity data were useful for constraining postseismic processes consistent with biviscous relaxation [*Han et al.*, 2008; *Panet et al.*, 2010; *Hoechner et al.*, 2011].

It is imperative to constrain the complex response of the Earth to the 2011 Tohoku-Oki earthquake to understand the rheology of the crust and mantle and the cycle of strain accumulation and release, ultimately, in order to estimate the subsequent seismic hazards in the surrounding region [*Wang et al.*, 2012a]. To this

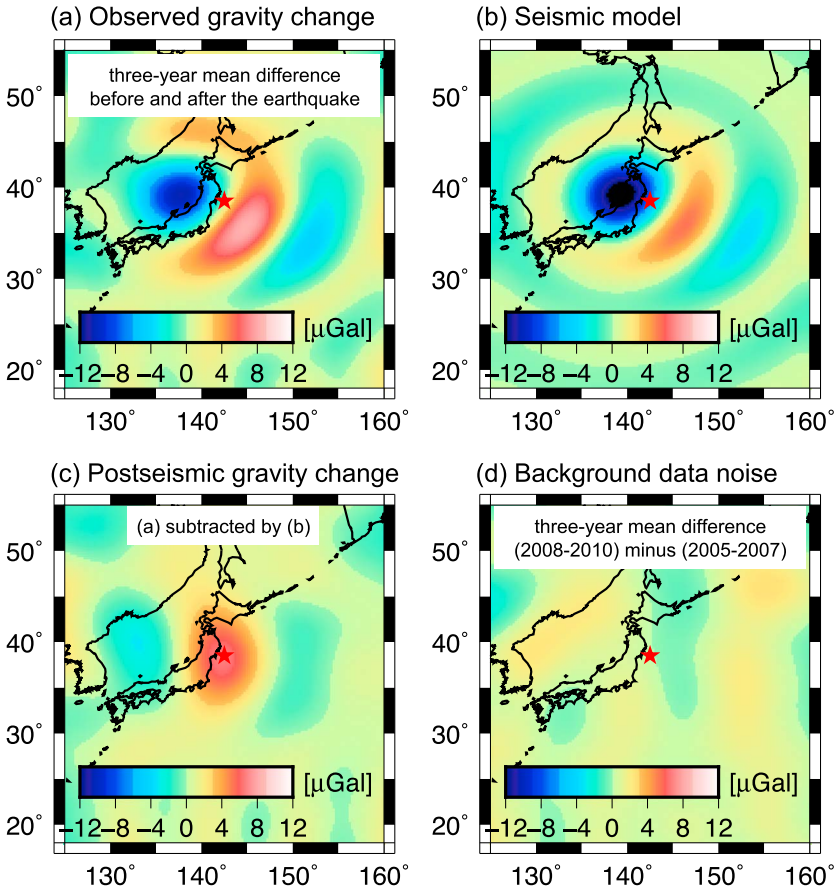

Figure 1. (a) The GRACE observed gravity change following the 2011 Tohoku-Oki earthquake computed by differencing the 3 year mean field before and after the earthquake. (b) The average synthetic gravity change caused by the coseismic deformation computed using four seismic models. (c) The postseismic GRACE gravity change computed by subtracting the seismic model prediction shown in Figure 1b from the mean difference field shown in Figure 1a. (d) The same as Figure 1a but during the 3 years between 2008–2010 and 2005–2007 (no large earthquake in-between).

end, we analyzed spatially and temporally continuous GRACE gravity observations implying the broadscale (~500 km) deformation of the surface and interior in response to regional-scale postearthquake stress/strain redistribution and evaluated two alternate postseismic processes of viscoelastic relaxation and afterslip. We document the rheology of the Earth inferred from the postseismic GRACE gravity data. Additionally, we calculated the high-resolution gravimetric response to this event and used these results with other available geodetic data to further discriminate between alternate mechanisms.

2. Postseismic Gravity Change From GRACE

We analyzed a total of 11 years of GRACE gravity data from 2003 to 2013 using the RL05 Level-2 (L2) monthly data products generated by Center for Space Research, University of Texas [*Tapley et al.*, 2004]. The March 2011 data were not used since the earthquake occurred in the middle of that month. The spherical harmonic coefficients up to degree and order 40 were used to represent gravity variations at a spatial resolution of 500 km, which is a conservative estimate of the GRACE data resolution. We first determined an analytical model of annual and semiannual sinusoids and a linear trend in the GRACE data by fitting the model to the monthly GRACE time series from January 2003 to February 2011 (i.e., prior to the earthquake). We extended the estimated trend out to the end of 2013 and removed it from the entire set of GRACE data before the analysis.

Figure 1a presents the GRACE gravity changes calculated by subtracting the mean gravity field over a preearthquake period (February 2008 to February 2011) from the mean field over a postearthquake period (April 2011 to December 2013). Therefore, it illustrates the coseismic deformation as well as the postseismic

deformation averaged over a period from 11 March 2011 to December 2013. Next, we computed the average coseismic gravity changes (Figure 1b) using the seismic centroid moment tensor (CMT) solutions (Global CMT and U.S. Geological Survey W-phase moment tensor) and two seismic finite fault models, Models II and III, from *Shao et al.* [2011]. They differ generally by 1–2 μGal at a spatial resolution of 500 km. The finite fault models we used present the largest slip updip of the hypocenter close to the trench consistent with the recent analysis including tsunami and seafloor data presenting the rupture out to the trench [*Lay et al.*, 2011; *Iinuma et al.*, 2012; *Hooper et al.*, 2013]. The dominant negative anomaly found in the seismic models indicates extensive crustal density decrease by volume extension under the influence of the ocean mass redistribution [*Han et al.*, 2006, 2013; *de Linage et al.*, 2009; *Broerse et al.*, 2011; *Cambiotti et al.*, 2011].

Figure 1c elucidates the postseismic gravity change computed by removing the coseismic (elastic) contribution (Figure 1b) from the GRACE data (Figure 1a). It indicates that the magnitude of postseismic deformation is a fraction of the coseismic deformation. During the first 3 years after the main shock, on average, 6 μGal of postseismic gravity change was estimated mostly around the epicenter. During a time period that does not include the perturbation due to a large earthquake (for example, the 2008–2010 mean field minus the 2005–2007 mean field), the mean field difference is within ±2 μGal (Figure 1d)—a measure of GRACE data noise and inherent gravity variations in this region. While the coseismic gravity change produced the positive anomaly offshore and the stronger negative anomaly landward, the postseismic gravity change yielded the positive anomaly prominently around the epicenter where the coseismic perturbation was small. To understand this, we further examine the temporal dependence of the postseismic gravity data and compare it with models of viscoelastic relaxation and afterslip.

3. Temporal Pattern of the Gravity Change From GRACE and Viscoelastic Relaxation

The temporal characteristics of postseismic gravity changes provide constraints on the physical processes and the rheological structure of the Earth. In particular, *Pollitz* [1997b] found that asthenospheric viscosity controls the temporal pattern of long-wavelength postseismic relaxation following a large megathrust event. Using the global normal mode formalism and viscous relaxation theory given in *Pollitz* [1997b] and the fault geometry notation of *Kanamori and Cipar* [1974, Figure 10] and *Kanamori and Given* [1981, Figure 1], we express the gravitational potential change induced by earthquake as follows:

$$g(\theta,\phi,t) = \left(\frac{-M_{rr}}{2}\right) g_{Mrr}(\theta,\phi,t) + (M_{r\theta}) g_{Mr\theta}(\theta,\phi,t) + (M_{r\phi}) g_{Mr\phi}(\theta,\phi,t) + \left(\frac{M_{\theta\theta}-M_{\phi\phi}}{2}\right) g_{M\theta\theta-M\phi\phi}(\theta,\phi,t) + (M_{\theta\phi}) g_{M\theta\phi}(\theta,\phi,t), \quad (1)$$

where a point dislocation source is at the (North) pole and described with the moment tensor components, M_{rr}, $M_{r\theta}$, $M_{r\phi}$, $M_{\theta\theta}-M_{\phi\phi}$, and, $M_{\theta\phi}$. The five independent and orthogonal basis functions of the earthquake geopotential change, g_{Mrr}, $g_{Mr\theta}$, $g_{Mr\phi}$, $g_{M\theta\theta-M\phi\phi}$, and $g_{M\theta\phi}$, are excited by each moment tensor component with a physical dimension of m^2/s^2 per Nm. They are computed with the eigenfunctions of viscoelastic normal modes (*Pollitz* [1997b], *Pollitz et al.* [2006], and *Han et al.* [2013] for the elastic normal mode) (see the supporting information). They are dependent only on the Earth's viscoelastic structure (i.e., precomputable regardless of seismic sources). The examples of the spatial pattern of each function for the elastic response (evaluated at $t=0$) are shown in Figure 2 (left).

The temporal evolution of each gravity component, γ_{Mrr}, $\gamma_{Mr\theta}$, $\gamma_{Mr\phi}$, $\gamma_{M\theta\theta-M\phi\phi}$, and $\gamma_{M\theta\phi}$, are simply obtained by the inner product of each basis function (e.g., g_{Mrr}) and the GRACE gravity data over unit sphere (see the supporting information for the explicit forms). The observed temporal changes from GRACE are presented in Figure 2 (right). The gravity changes corresponding to the moment tensor components of $M_{r\theta}$ and $M_{\theta\phi}$ can be resolved with the highest accuracy of $20–30\times10^{20}$ Nm (or $M_w = 8.2–8.3$), while the other components have the accuracy of 80×10^{20} Nm (or $M_w = 8.6$). The north-south sampling nature of the GRACE intersatellite tracking enables the best sensitivity in estimation of $M_{r\theta}$ and $M_{\theta\phi}$ components, 3–4 times better than other components. This indicates the GRACE's sensitivity to earthquakes as small as $M_w = 8.2$ in this region, depending on the focal mechanism.

The average and standard deviation of four seismic models are shown as thick black solid and thin black dashed lines in Figure 2, respectively. The first few months of GRACE data after the earthquake agree with the coseismic

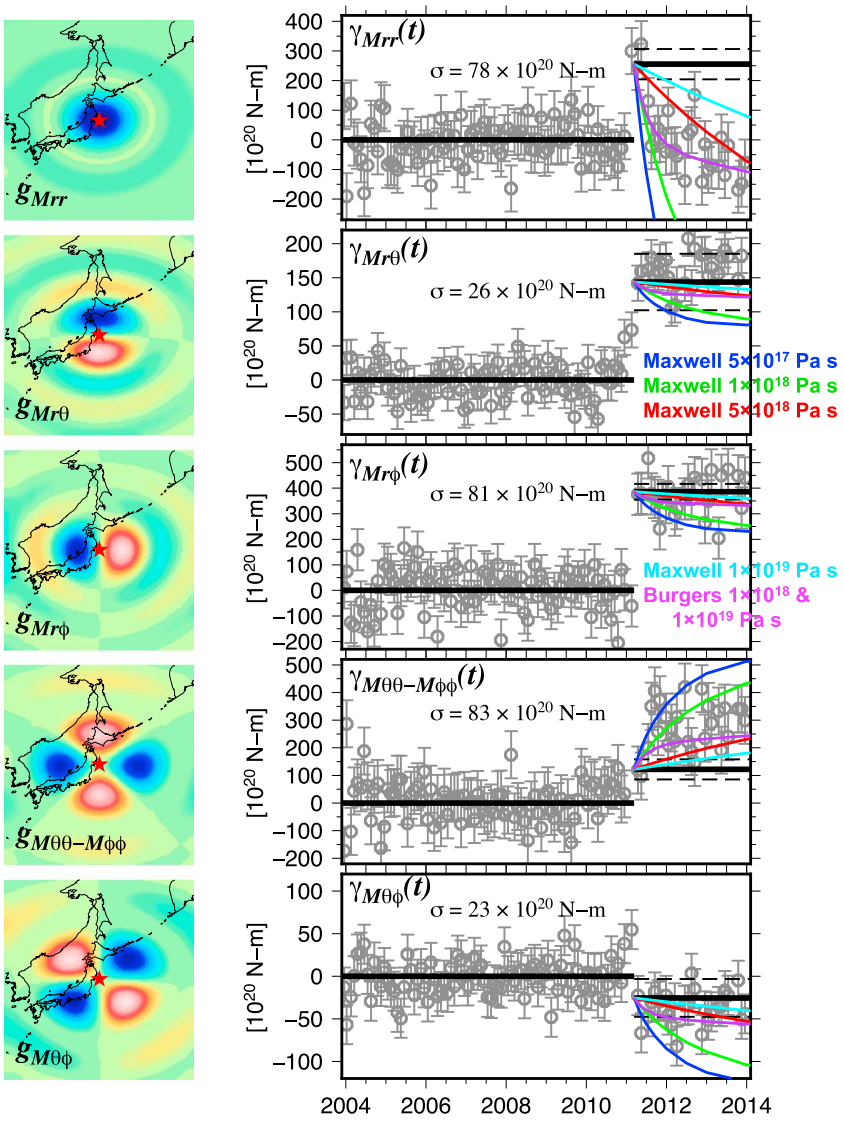

Figure 2. (left) The spatial patterns of the gravity changes to be excited by five independent moment tensor components of M_{rr}, $M_{r\theta}$, $M_{r\phi}$, $M_{\theta\theta} - M_{\phi\phi}$, and, $M_{\theta\phi}$, respectively. The exact scale is dependent on the moment tensor (the negative to positive values are depicted with blue to red colors). The coordinates of the dislocation source are 38.5°N, 142.6°E (depicted as a red star), and its depth is 20 km. (right) The corresponding temporal variations of each component of the gravity change before and after the earthquake. The GRACE observations are shown by gray circles with the error estimate. The mean value of the synthetic gravity changes computed from various seismic models is shown in thick black solid line, and the 1 sigma variation of the models is depicted in thin black dashed line. Depicted are viscoelastic gravity changes computed from the Maxwell asthenosphere model with the viscosity of 5×10^{17} Pa s (blue), 10^{18} Pa s (green), 5×10^{18} Pa s (red), and 10^{19} Pa s (cyan) and from the biviscous (Burgers body) asthenosphere model with transient viscosity of 10^{18} Pa s and steady state viscosity of 10^{19} Pa s (purple).

changes from seismic models; however, subsequently, there are substantial variations observed particularly in M_{rr} and $M_{\theta\theta} - M_{\phi\phi}$. There is no significant postseismic change discerned from other components. We compared such observations with theoretical models. We used a spherically stratified viscoelastic Earth model that includes a global ocean layer (3 km thick), an elastic lithosphere (60 km thick) overlying an asthenosphere extending to a depth of 220 km, and an upper (220–670 km) and lower (670–2891 km) mantle [*Pollitz et al.*, 2006]. The elastic thickness of 63 km near the Japan trench was estimated independently from the marine gravity and flexural analysis [*Levitt and Sandwell*, 1995]. The stratified density structure is consistent with Preliminary Reference Earth Model [*Dziewonski and Anderson*, 1981]. The upper and lower mantle was modeled with a Maxwell rheology with the viscosity of 10^{20} Pa s and 10^{21} Pa s, respectively. We tested five different

rheological models for the asthenosphere; (1) Maxwell viscosity of 5×10^{17} Pa s, (2) 10^{18} Pa s, (3) 5×10^{18} Pa s, (4) 10^{19} Pa s, and finally, (5) transient (Kelvin) viscosity of 10^{18} Pa s and steady state (Maxwell) viscosity of 10^{19} Pa s with biviscous (Burgers body) rheology [*Ivins and Sammis*, 1996]. The ratio between Kelvin and Maxwell rigidity is assumed to be 1. The lithosphere overlying the asthenosphere is assumed to be elastic by assigning a very large viscosity of 10^{30} Pa s. We use the computer code VISCO1D [*Pollitz*, 1997b] and its modification to compute the postseismic gravity response to a dislocation source for alternate spherical viscoelastic models [*Pollitz*, 1997a; *Pollitz et al.*, 2006]. The *Pollitz* [1997b] method is applicable to any deformation field represented as a viscoelastic normal mode sum on a laterally homogeneous spherical model, specifically, a weighted spherical harmonic sum of displacement-stress vectors. Although originally designed for the case of static gravity changes, it is also directly applicable to the case of postseismic gravity changes by employing equation (21) of *Pollitz* [1997a] as the viscoelastic normal mode sum.

Figure 2 presents the various synthetic viscoelastic gravity changes, depicted in solid colored curves. These viscoelastic simulations were computed with the CMT solution obtained from *Han et al.* [2013]. The equivalent simulations with a finite fault model such as Model II of *Shao et al.* [2011] are shown in the Figure S1 in the supporting information, and they are not different significantly at the spatial scale of consideration because of the concentrated coseismic slip of this earthquake. For the components M_{rr} and $M_{\theta\theta} - M_{\phi\phi}$, the model runs with the asthenospheric Maxwell viscosity of 5×10^{17} and 10^{18} Pa s (blue and green curves, respectively) predict rapid gravity change within a few months after the main shock. This may be reconciled with the short-term GRACE observations; however, the long-term changes with these viscosities are predicted to be overly large. The simulations with the asthenospheric Maxwell viscosity of 5×10^{18} and 10^{19} Pa s (red and cyan curves, respectively) do not reproduce the rapid change observed during the first few months but capture the cumulative long-term change. The rapid change followed by gradual variation in the GRACE gravity data are best reproduced with the biviscous relaxation model with the transient viscosity of 10^{18} Pa s and steady state viscosity of 10^{19} Pa s (purple). For the other components of $M_{r\theta}$, $M_{r\phi}$, and $M_{\theta\phi}$ that do not show discernible postseismic gravity change observation, any model with the steady state viscosity smaller than 5×10^{18} Pa s is ruled out. Overall, the biviscous asthenospheric model satisfactorily explains the postseismic gravity changes observed by GRACE, similar to the findings for the 2004 Sumatra-Andaman earthquake [*Pollitz et al.*, 2006; *Han et al.*, 2008; *Panet et al.*, 2010; *Hoechner et al.*, 2011].

4. Postseismic Gravity Change Compared to Afterslip

Alternatively, the afterslip on the coseismic rupture surface and its downdip extension is also a viable candidate to explain postseismic deformation after large megathrust earthquakes. We use the finite fault models of afterslip to quantify the predicted gravity for comparison with the time series of GRACE gravity data. The (kinematic) afterslip model was constrained by GPS measurements of postseismic displacement accumulated over various intervals (7, 20, 48, 107, 200, 289, 381, and 564 days) up to the 1.5 years after the main shock, assuming that the postseismic displacement is entirely due to afterslip [*Diao et al.*, 2013]. The maximum cumulative slip of 4 m over the period of 1.5 years and the equivalent seismic moment of 2.3×10^{22} Nm was found by elastic dislocation modeling of postseismic GPS data [*Ozawa et al.*, 2011; *Diao et al.*, 2013]. For the time intervals given above, we calculated the deformation associated with afterslip using dislocation theory [e.g., *Cohen*, 1999].

Figure 3a presents the GRACE postseismic gravity data (same as Figure 1c), and three different locations where the positive and negative (to a lesser extent) gravity changes are identified. The gravity change of the M_{rr} component is responsible mostly for the positive gravity at P_2, while the one of $M_{\theta\theta} - M_{\phi\phi}$ is for the negative gravity change at P_1 and P_3. The GRACE gravity time series at each location are presented with the error estimates of 2 μGal in Figure 3b. The elastic gravity change was computed with Model II of *Shao et al.* [2011], and the viscoelastic gravity change was computed using the same seismic source model and the biviscous Earth's model characterized with the transient viscosity of 10^{18} Pa s and steady state viscosity of 10^{19} Pa s for the asthenosphere. The time series of the afterslip gravity change from the finite fault model of *Diao et al.* [2013] is also shown in Figure 3b at three different locations.

The snapshot of the synthetic gravity change 1 year after the main shock is depicted in Figures 3c and 3d, respectively, for the viscoelastic relaxation and the afterslip models. Both postseismic processes produce similar gravity change in spatial and temporal pattern as well as the magnitude. The positive anomaly

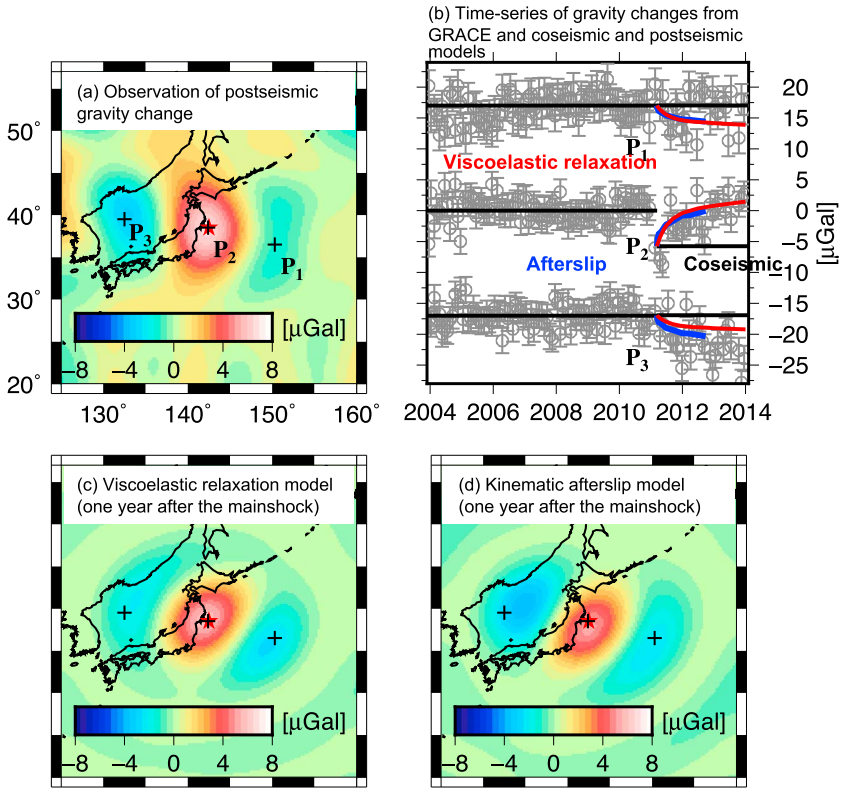

Figure 3. (a) GRACE observation of postseismic gravity change (same as Figure 1c). (b) Time series of the GRACE gravity change at P_1, P_2, and P_3. An arbitrary bias of 17 and −17 μGal was added to the ones of P_1 and P_3, respectively, for plotting clarity. The model prediction of coseismic slip, afterslip, and viscoelastic relaxation is shown, respectively, as black, blue, and red lines. (c) A snapshot of postseismic gravity change 1 year after the main shock from the viscoelastic relaxation model. (d) Same as Figure 3c but from the afterslip model.

around the epicenter (P_2) is a dominant feature consistently found in the GRACE measurements and in both viscoelastic relaxation and afterslip models. The secondary anomalies with 3–4 times smaller magnitude are the negative changes in the west and the east of the positive anomaly (P_3 and P_1, respectively). The afterslip model predicts a slightly larger anomaly in the west than the one in the east.

5. Discussion

So far, we examined the postseismic "free-air" gravity changes measured from GRACE and computed from viscoelastic relaxation and afterslip models at a spatial resolution of 500 km; it is difficult to discriminate these competing postseismic processes from the GRACE data alone for the period of a couple of years after the main shock. In order to further understand gravity change and deformation associated with these postseismic mechanisms, we computed the gravity effect of surface vertical deformation (uplift/subsidence of the ocean-seafloor interface) and interior deformation (Bouguer gravity anomaly) separately [*Han et al.*, 2006].

The gravity change of seafloor vertical motion by viscoelastic relaxation (Figure 4a) is characterized by a dominant positive anomaly around the epicenter implying broadscale (500 km) seafloor uplift. The Bouguer anomaly of viscoelastic relaxation (Figure 4b), computed by subtracting the effect of seafloor vertical motion from the free-air anomaly, shows a similar pattern of gravity change but with a magnitude 2–3 times smaller. The Bouguer gravity change is explained mostly by vertical deformation of the density interfaces of the upper and lower crust and of the crust and upper mantle (Moho). It indicates that the broadscale uplift gradually occurs with negligible change in bulk volume (or density) as viscous asthenosphere and mantle yield to the coseismic stresses. This is distinctly different from the coseismic deformation involving significant density change.

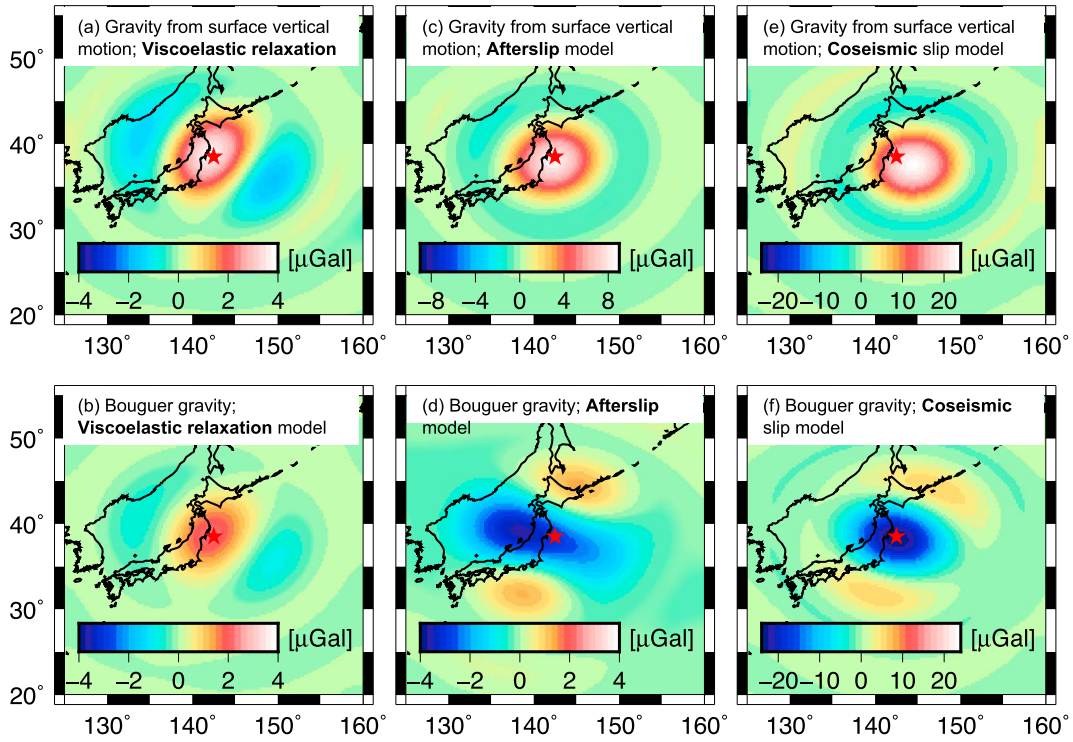

Figure 4. (a, c, and e) Gravity change due to seafloor vertical motion computed, respectively, from biviscous viscoelastic relaxation, afterslip, and coseismic slip. (b, d, and f) Same as Figures 4a, 4c, and 4e, respectively, but for the Bouguer gravity.

In comparison to the uplift by viscoelastic relaxation, the afterslip model predicts twice larger seafloor uplift around the epicenter as highlighted by the doubled magnitude of the positive gravity (Figure 4c). The Bouguer gravity of afterslip (Figure 4d) is characterized by a negative anomaly orthogonal to the strike direction. This negative anomaly is primarily due to volume expansion or dilatation associated with the downdip afterslip within the lower crust and the upper mantle. We also computed the gravity changes of seafloor vertical motion and Bouguer anomaly (Figures 4e and 4f, respectively) from the coseismic slip model, Model II of *Shao et al.* [2011].

The majority of the coseismic slip is estimated at the top 25 km of the crustal layer, while the afterslip is concentrated mostly at depths of 40–50 km [*Ozawa et al.*, 2011; *Diao et al.*, 2013]. Deeper sources like the downdip afterslip yield smaller volume change due to larger rigidity and bulk modulus at the mantle depth, while shallower coseismic slip associated with smaller rigidity and bulk modulus at the crustal depth yields larger volume change. As a result, distinct patterns of gravity changes are produced by afterslip and coseismic slip. The deep afterslip produces the smaller Bouguer gravity anomaly (Figure 4d) relative to the gravity from seafloor vertical deformation (Figure 4c) and thus results in the smaller negative change in the free-air gravity (Figure 3d). On the other hand, the coseismic Bouguer gravity anomaly (Figure 4f) is as large as the coseismic vertical displacement (Figure 4e), which reduces the positive contribution to the free-air gravity (Figure 1b). The downdip afterslip also moves the peak gravity change landward (west), relative to the coseismic gravity change.

We repeated the same calculations of synthetic gravity changes for the viscoelastic, afterslip, and coseismic deformation but at a resolution of 55 km by extending the spherical harmonic degree and order up to 360 and by using a finite fault model *Shao et al.* [2011] (shown in Figure S2 in the supporting information). We found that the high degree expansion of the viscoelastic simulation predicts local subsidence superimposed on the broadscale uplift across the Japan trench. While the east coast of the island and the east of the trench undergo uplift, the area localized above the rupture zone undergoes subsidence, as implied by the positive and negative gravity change, respectively. This is the very characteristic pattern of surface vertical motion followed by thrust earthquakes when the elastic lithosphere overlying the viscoelastic asthenosphere is only "partially" ruptured

[*Melosh*, 1983; *Cohen*, 1999]. *Melosh* [1983] found that the top boundary of the viscous asthenosphere experiences local extension beneath the fault if the fault stops within the lithosphere, which causes the local subsidence on top of regional uplift. However, if the fault cuts through the lithosphere, the boundary of the asthenosphere is subject to net shortening and the surface undergoes uplift.

Sato et al. [2013], *Burgmann et al.* [2014], and *Hu et al.* [2014] reported the postseismic subsidence of the seafloor above the rupture zone by a few decimeters within a couple of years after the main shock using the GPS-acoustic positioning and seafloor pressure data, while the GPS data implied postseismic uplift along the coast by a few centimeters [*Japan Coast Guard*, 2012; *Japan Coast Guard and Tohoku University*, 2013]. Such subsidence may yield tens of μGal gravity decrease (−7 μGal per 10 cm of seafloor subsidence; the Bouguer correction with the density contrast between the crust and ocean). No seafloor measurement is available in the Pacific Plate, to the east of the trench, where viscoelastic uplift is predicted. The local subsidence from the viscoelastic model is diminished by the uplift in the periphery of the overthrust and underthrust blocks at a broadscale resolution, which is what the GRACE data observed. In contrast, the downdip afterslip model such as *Diao et al.* [2013] does not produce subsidence, although the model is consistent with onland postseismic GPS motions. *Kogan et al.* [2011] reported such inconsistency in the postseismic vertical motion from afterslip following the great 2006 and 2007 Kuril earthquakes. *Hu et al.* [2014] found that the poroelastic rebound may yield uplift above the rupture zone by a few decimeters in 2 years. Although all of these postseismic processes are likely present and compensate each other at times, we hypothesize the viscoelastic relaxation triggered by the partially ruptured elastic lithosphere is a main driver of the local subsidence above the rupture region.

6. Conclusion

GRACE observed postseismic gravity increase by 6 μGal (40–50% of the coseismic gravity change) within a couple of years after the 2011 Tohoku-Oki earthquake. The postseismic free-air gravity changes from viscoelastic relaxation and afterslip are similar at the scale of 500 km commensurate with the GRACE data resolution. However, the Bouguer gravity responses are distinct; the Bouguer anomaly of viscoelastic relaxation is positively correlated with the free-air anomaly, while the Bouguer anomaly of afterslip is negatively correlated. The broadscale postseismic gravity observation and the local subsidence measurement above the rupture zone are consistent with a biviscous viscoelastic flow model. The viscosity is the most important factor to govern evolution of the long-wavelength stress field after the earthquake. Large-scale monitoring of the postseismic deformation (gravity as well as vertical displacement) will help characterize the rheological properties of the Earth's interior that may lead to a better understanding of increased seismic hazard following great earthquakes.

Acknowledgments

This work was supported by NASA's GRACE project and Earth Surface and Interior program. We thank Riccardo Riva for sharing computer codes for the normal mode analysis, Roland Burgmann and Yan Hu for sharing their postseismic modeling and analysis, Faqi Diao for providing the finite fault models of afterslip, and an anonymous reviewer and M. Kogan for their constructive comments. The GRACE data for this paper are available at http://podaac.jpl.nasa.gov/GRACE.

The Editor thanks Mikhail Kogan and an anonymous reviewer for their assistance in evaluating this paper.

References

Broerse, D. B. T., L. L. A. Vermeersen, R. E. M. Riva, and W. van der Wal (2011), Ocean contribution to co-seismic crustal deformation and geoid anomalies: Application to the 2004 December 26 Sumatran-Andaman earthquake, *Earth Planet. Sci. Lett.*, *305*, 341–349, doi:10.1016/j.epsl.2011.03.011.

Burgmann, R., et al. (2014), Time-dependent crustal deformation and slip following the 2011 M9 Tohoku earthquake, paper presented at UNAVCO Science Workshop, Broomfield, Colo., 4–6 Mar.

Cambiotti, G., and R. Sabadini (2012), A source model for the great 2011 Tohoku earthquake (MW = 9.1) from inversion of GRACE gravity data, *Earth Planet. Sci. Lett.*, *335*, 72–79, doi:10.1016/j.epsl.2012.05.002.

Cambiotti, G., and R. Sabadini (2013), Gravitational seismology retrieving Centroid-Moment-Tensor solution of the 2011 Tohoku earthquake, *J. Geophys. Res. Solid Earth*, *118*, 183–194, doi:10.1029/2012JB009555.

Cambiotti, G., A. Bordoni, R. Sabadini, and L. Colli (2011), GRACE gravity data help constraining seismic models of the 2004 Sumatran earthquake, *J. Geophys. Res.*, *116*, B10403, doi:10.1029/2010JB007848.

Cohen, S. (1999), Numerical models of crustal deformation in seismic zones, *Adv. Geophys.*, *41*, 133–231.

de Linage, C., L. Rivera, J. Hinderer, J.-P. Boy, Y. Rogister, S. Lambotte, and R. Biancale (2009), Separation of coseismic and postseismic gravity changes for the 2004 Sumatra-Andaman earthquake from 4.6 yr of GRACE observations and modelling of the coseismic change by normal-modes summation, *Geophy. J. Int.*, *176*, 695–714.

Diao, F., X. Xiong, R. Wang, Y. Zheng, T. R. Walter, H. Weng, and J. Li (2013), Overlapping post-seismic deformation processes: Afterslip and viscoelastic relaxation following the 2011 Mw 9.0 Tohoku (Japan) earthquake, *Geophys. J. Int.*, doi:10.1093/gji/ggt376.

Dziewonski, A. M., and D. L. Anderson (1981), Preliminary reference Earth model, *Phys. Earth Planet. Inter.*, *25*, 297–356.

Han, S.-C., C. K. Shum, M. Bevis, C. Ji, and C.-Y. Kuo (2006), Crustal dilatation observed by GRACE after the 2004 Sumatra-Andaman earth- quake, *Science*, *313*, 658–662, doi:10.1126/science.1128661.

Han, S.-C., J. Sauber, S. Luthcke, C. Ji, and F. Pollitz (2008), Implications of postseismic gravity change following the great 2004 Sumatra-Andaman earthquake from the regional harmonic analysis of GRACE intersatellite tracking data, *J. Geophys. Res.*, *113*, B11413, doi:10.1029/2008JB005705.

Han, S.-C., J. Sauber, and R. Riva (2011), Contribution of satellite gravimetry to understanding seismic source processes of the 2011 Tohoku-Oki earthquake, *Geophys. Res. Lett.*, *38*, L24312, doi:10.1029/2011GL049975.

Han, S.-C., R. Riva, J. Sauber, and E. Okal (2013), Source parameter inversion for recent great earthquakes from a decade-long observation of global gravity fields, *J. Geophys. Res. Solid Earth*, *118*, 1240–1267, doi:10.1002/jgrb.50116.

Hoechner, A., S. V. Sobolev, I. Einarsson, and R. Wang (2011), Investigation on afterslip and steady state and transient rheology based on postseismic deformation and geoid change caused by the Sumatra 2004 earthquake, *Geochem. Geophys. Geosyst.*, *12*, Q07010, doi:10.1029/2010GC003450.

Hooper, A., et al. (2013), Importance of horizontal seafloor motion on tsunami height for the 2011 Mw = 9.0 Tohoku-Oki earthquake, *Earth Planet. Sci. Lett.*, *361*, 469–479, doi:10.1016/j.epsl.2012.11.013.

Hu, Y., R. Burgmann, J. Freymueller, P. Banerjee, N. Uchida, T. Matsuzawa, and K. Wang (2014), Contributions of upper mantle rheology, afterslip and poroelasticity to the viscoelastic postseismic deformation of the 2011 Tohoku earthquake, paper presented at Crustal Deformation Modeling workshop, Stanford, Calif., 23–27 June. [Available at http://geodynamics.org/cig/files/7814/0372/1199/CDM2014_YanHu.pdf.]

Iinuma, T., et al. (2012), Coseismic slip distribution of the 2011 off the Pacific Coast of Tohoku Earthquake (M9.0) refined by means of seafloor geodetic data, *J. Geophys. Res.*, *117*, B07409, doi:10.1029/2012JB009186.

Ivins, E. R., and C. G. Sammis (1996), Transient creep of a composite lower crust: 1. Constitutive theory, *J. Geophys. Res.*, *101*, 27,981–28,004, doi:10.1029/96JB02847.

Japan Coast Guard (2012), Seafloor movements obtained by seafloor geodetic observations after the 2011 off the Pacific Coast of Tohoku earthquake [In Japanese], *Rep. Coord. Comm. Earthq. Predict.*, *88*, 150–154.

Japan Coast Guard, and Tohoku University (2013), Seafloor movements observed by seafloor geodetic observations after the 2011 off the Pacific coast of Tohoku Earthquake, Report of the Coordinating Committee for Earthquake Prediction, Japan, 90, 3-4. [Available at http://cais.gsi.go.jp/YOCHIREN/activity/194/194.html.]

Kanamori, H., and J. J. Cipar (1974), Focal process of the great Chilean earthquake, May 22, 1960, *Phys. Earth Planet. Inter.*, *9*, 128–136.

Kanamori, H., and J. W. Given (1981), Use of long-period surface waves for rapid determination of earthquake source parameters, *Phys. Earth Planet. Int.*, *27*, 8–31.

Kogan, M., N. F. Vasilenko, D. I. Frolov, J. T. Freymueller, G. M. Steblov, B. W. Levin, and A. S. Prytkov (2011), The mechanism of postseismic deformation triggered by the 2006–2007 great Kuril earthquakes, *Geophys. Res. Lett.*, *38*, L06304, doi:10.1029/2011GL046855.

Lay, T., C. J. Ammon, H. Kanamori, L. Xue, and M. J. Kim (2011), Possible large near-trench slip during the 2011 Mw 9. 0 off the Pacific Coast of Tohoku Earthquake, *Earth Planets Space*, *63*(7), 687692, doi:10.5047/eps.2011.05.033.

Levitt, D. A., and D. T. Sandwell (1995), Lithospheric bending at subduction zones based on depth soundings and satellite gravity, *J. Geophys. Res.*, *100*, 379–400, doi:10.1029/94JB02468.

Matsuo, K., and K. Heki (2011), Coseismic gravity changes of the 2011 Tohoku-Oki earthquake from satellite gravimetry, *Geophys. Res. Lett.*, *38*, L00G12, doi:10.1029/2011GL049018.

Melosh, H. J. (1983), Vertical movements following a dip-slip earthquake, *Geophys. Res. Lett.*, *10*, 47–50, doi:10.1029/GL010i001p00047.

Ozawa, S., T. Nishimura, H. Suito, T. Kobayashi, M. Tobita, and T. Imakiire (2011), Coseismic and postseismic slip of the 2011 magnitude-9 Tohoku-Oki earthquake, *Nature*, *475*, 373–376, doi:10.1038/nature10227.

Panet, I., F. Pollitz, V. Mikhailov, M. Diament, P. Banerjee, and K. Grijalva (2010), Upper mantle rheology from GRACE and GPS postseismic deformation after the 2004 Sumatra-Andaman earthquake, *Geochem. Geophys. Geosyst.*, *11*, Q06008, doi:10.1029/2009GC002905.

Pollitz, F. F. (1997a), Gravity anomaly from faulting on a layered spherical earth with application to central Japan, *Phys. Earth Planet. Int.*, *99*, 259–271.

Pollitz, F. F. (1997b), Gravitational-viscoelestic postseismic relaxation on a layered spherical Earth, *J. Geophys. Res.*, *102*, 17,921–17,941, doi:10.1029/97JB01277.

Pollitz, F., R. Bürgmann, and P. Banerjee (2006), Postseismic relaxation following the great 2004 Sumatra-Andaman earthquake on a compressible self-gravitating Earth, *Geophys. J. Int.*, *167*, 397–420.

Sato, M., T. Ishikawa, N. Ujihara, S. Yoshida, M. Fujita, M. Mochizuki, and A. Asada (2011), Displacement above the hypocenter of the 2011 Tohoku-Oki earthquake, *Science*, *332*, 1395, doi:10.1126/science.1207401.

Sato, M., S. Watanabe, Y. Yokota, N. Ujihara, T. Ishikawa, M. Fujita, M. Mochizuki, and A. Asada (2013), Postseismic seafloor movements above the focal region of the 2011 Tohoku-Oki earthquake, Abstract G11B-0920 presented at 2013 Fall Meeting, AGU, San Francisco, Calif., 9-13 Dec.

Shao, G., X. Li, C. Ji, and T. Maeda (2011), Focal mechanism and slip history of 2011 Mw 9.1 off the Pacific coast of Tohoku Earthquake, constrained with teleseismic body and surface waves, *Earth Planets Space*, *63*, 559–564.

Simons, M., et al. (2011), The 2011 magnitude 9.0 Tohoku-Oki earthquake: Mosaicking the megathrust from seconds to centuries, *Science*, *332*, 1421.

Tapley, B. D., S. Bettadpur, J. Ries, P. Thompson, and M. Watkins (2004), GRACE measurements of mass variability in the Earth system, *Science*, *305*, 503–505, doi:10.1126/science.1099192.

Wang, K., Y. Hu, and J. He (2012a), Deformation cycles of subduction earthquakes in a viscoelastic Earth, *Nature*, *484*, 327–332, doi:10.1038/nature11032.

Wang, L., C. K. Shum, F. J. Simons, B. Tapley, and C. Dai (2012b), Coseismic and postseismic deformation of the 2011 Tohoku-Oki earthquake constrained by GRACE gravimetry, *Geophys. Res. Lett.*, *39*, L07301, doi:10.1029/2012GL051104